X-ray photoemission studies of the metal-insulator transition in LaAlO$_3$/SrTiO$_3$ structures grown by molecular beam epitaxy

Y. Segal,[*] J. H. Ngai, J. W. Reiner, F. J. Walker, and C. H. Ahn

Department of Applied Physics, Yale University, New Haven, Connecticut 06520-8284, USA

(Received 16 September 2009; revised manuscript received 8 November 2009; published 23 December 2009)

LaAlO$_3$/SrTiO$_3$ interfaces grown by molecular beam epitaxy show a metal-insulator transition at a critical film thickness of four unit cells of LaAlO$_3$ on TiO$_2$-terminated SrTiO$_3$ substrates. This transition had previously been observed in LaAlO$_3$ films grown by pulsed laser deposition, where defects related to the growth process have been suggested as playing a role in the interface behavior. X-ray photoemission was used to examine the band offsets and look for an electric field across LaAlO$_3$ for a range of film thicknesses on both SrO- and TiO$_2$-terminated SrTiO$_3$ substrates. These results are compared to the predictions of the polar catastrophe model for the emergence of a metallic interface in this system. We do not find the predicted electric field in the LaAlO$_3$ or any dependence on substrate termination. While the observation of metal-insulator transitions in LaAlO$_3$/SrTiO$_3$ structures grown by different techniques points to an intrinsic effect, the absence of an electric field in the LaAlO$_3$ layer is not consistent with the polar catastrophe model of interface metallicity.

The LaAlO$_3$ (LAO)/SrTiO$_3$ (STO) system has drawn an exceptional amount of interest due to its transport properties,[1,2] which are associated with the existence of an electron gas localized near the interface. However, the origin of the electron gas, emerging at the interface between two band insulators, is still under debate. A key feature of transport in this system is its dependence on STO substrate termination and LAO film thickness. Interfaces grown on TiO$_2$-terminated STO show no conductivity when the LAO film is thinner than four unit cells (uc); however, a sharp transition to metallic conductivity appears upon adding a single unit cell to the film.[3] Interfaces grown on SrO-terminated STO are insulating[4] for all LAO thicknesses. To explain the observed conductivity, both extrinsic and intrinsic mechanisms have been invoked for doping near the interface. Doping of the STO via oxygen vacancies created during growth can lead to metallic conductivity.[5] If these vacancies are filled, intrinsic mechanisms become dominant. The greatest amount of theoretical attention has been focused on the polar discontinuity between the two oxides.[6–10] STO planes are formally neutral, while LAO planes have an alternating $\pm e$ charge. Calculations show that, if the interface is abrupt, the charge discontinuity creates a built-in field in the LAO film. The potential drop across the film grows until it is large enough to cause an injection of carriers from the surface to the interface. A different mechanism put forward involves intermixing of the two oxides.[11,12]

In this work we experimentally investigate both the extrinsic and intrinsic pathways using thin films grown by molecular beam epitaxy (MBE). Previous experimental work on this system has been done on films formed via pulsed laser deposition (PLD). The use of MBE is important because the high kinetic energy of evaporants inherent to the ablation process of PLD can induce defects in the STO layers,[1] similar to the effect of Ar$^+$ irradiation.[13] Evaporants in MBE, however, have thermal energies on the order of 0.1 eV.

We investigate intrinsic doping mechanisms using x-ray photoelectron spectroscopy (XPS). Core-level photoemission is particularly useful when looking for the electric field in the LAO film, as predicted by the polar catastrophe picture. Built-in electric fields manifest themselves as shifts of the film's core-level emission with film thickness. This type of analysis was used to detect the field in Al$_x$Ga$_{1-x}$N heterointerfaces,[14] where a polarization discontinuity leads to two-dimensional electron gas formation. The magnitude of the predicted fields in the LAO/STO system [0.6–0.9 V/uc (Refs. 7 and 8) and higher[6]] should manifest itself in an easily observed core-level shift and broadening, reflecting the metal-insulator transition and substrate termination dependence. We note that previous photoemission studies of this system[15,16] looked at substrate photoemission and do not provide a complete picture of the LAO/STO heterostructure.

Commercially available TiO$_2$-terminated 5×5 mm^2 STO substrates (Crystech Gmbh) were introduced into an oxide MBE chamber with a 1×10^{-10} Torr base pressure. Effusion cells containing elemental Sr, La, and Al were used to thermally evaporate the metals onto the substrate, where they react with molecular oxygen introduced through a leak valve. Metal fluxes were measured using a quartz crystal monitor, with the thickness calibrated by counting reflection high-energy electron diffraction (RHEED) oscillations. The substrate temperature was kept at 675 °C and the O$_2$ partial pressure during deposition was $\sim 3 \times 10^{-7}$ Torr. Strong RHEED oscillations were observed, indicating a layer-by-layer growth mode of the films. Atomic force microscopy (AFM) characterization showed large smooth terraces (Fig. 1).

To study the conductivity transition, we characterize 2–9 uc films that were grown on TiO$_2$-terminated STO, and 3–7 uc films that were grown on SrO-terminated STO. The SrO termination was created by depositing one monolayer of Sr on TiO$_2$-terminated substrates in the presence of oxygen, in analogy to the PLD process.[4] Van der Pauw measurements were performed on these samples directly after growth and after an anneal at 350 °C under 75 cc/min of flowing oxygen for 90 h. This anneal was found to be sufficient to remove all
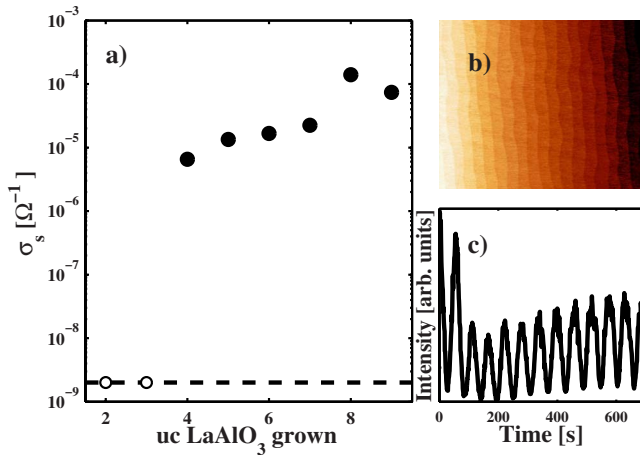
FIG. 1. (Color online) (a) Room-temperature conductivity of LAO/STO interfaces grown on TiO_2-terminated STO. The dashed line signifies the sensitivity limit of measurement. (b) 4×3 μm^2 AFM image of 5 uc LAO grown on TiO_2-terminated STO. (c) RHEED oscillations observed during LAO growth. The growth rate is 1 uc/min.

conductivity in the SrO-terminated samples, via removal of oxygen vacancies in the STO.

Transport measurements demonstrate the termination dependence and metal-insulator transition typical of this system. As-grown samples were reduced throughout the bulk of the STO, as evident by the sample's darkened color. The sheet charge density was about 10^{16} charges/cm^2, as seen under similar reducing conditions by other groups.[5] After annealing and storage in the dark, the conductivity of TiO_2-terminated samples above 4 uc of LAO showed metallic behavior, while 2 and 3 uc samples showed no measurable conductivity, confirming the metal-insulator transition at this thickness[3] (Fig. 1). Charge densities were $\sim 1 \times 10^{13} - 3 \times 10^{13}$ charges/cm^2, which is considered the intrinsic carrier density due to the interface.[3,5] LAO films grown on SrO termination show no measurable conductivity.[4] The thickness and termination dependence of these measurements establish the same phenomenology of the interface conductivity as observed for PLD-grown films.

XPS measurements were done using Mg $K\alpha$ photons, with electron emission normal to the surface. Samples were transferred through air to the XPS chamber. Analysis focuses on the substrate Sr $3d$ and film La $4d$ and Al $2p$ core-level peaks. We use relative peak separations and widths as our quantities of interest to cancel out the effect of charging and surface photovoltage. The La $4d$ peak contains two final states,[17] typical for lanthanum oxides. For separation and broadening comparisons, we use the 5/2-derived peak. The average full width half maximum (FWHM) of the Sr $3d_{5/2}$ remains unchanged after annealing, indicating that no peak broadening occurs due to inhomogeneous charging. Spin-orbit separations (Sr $3d_{5/2}$-$3d_{3/2}$, La $4d_{5/2}$-$4d_{3/2}$) were also unchanged. The theoretical attenuation length for the photo-emitted electrons in LAO, calculated using the TPP-2M formula[18] is 21.4 Å and is in good agreement with the observed attenuation of the substrate peak. Thick epitaxial films of LAO and STO on Si (Refs. 19 and 20) were used as
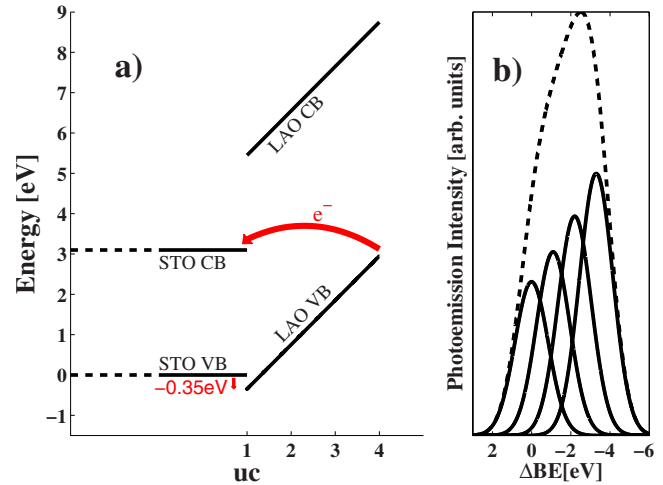

FIG. 2. (Color online) (a) Polar catastrophe model for the appearance of conductivity above 4 uc on TiO_2-terminated substrates. The LAO valence band bends upward until injection of electrons into the STO conduction band can occur. The subsequent downward bending of the STO bands is not shown. The experimentally determined valence-band offset is 0.35 eV. Band-gap values are from Refs. 21 and 22. (b) A schematic of a composite photoemission peak from the LAO core levels showing shift and broadening.

reference samples for valence-band-edge (VBE) positions. Separations of 130.90 ± 0.12 eV between the Sr $3d_{5/2}$ peak and the STO VBE and 99.80 ± 0.14 eV between the La $4d_{5/2}$ peak and the LAO VBE are found.[21]

In the polar catastrophe picture, a built-in field exists in the LAO due to the polar discontinuity of the buried interface. For the TiO_2-terminated case, the field points toward the surface, so that the LAO valence-band energy increases toward the surface (Fig. 2). The potential drop across the LAO grows with increasing film thickness, until the valence band at the surface becomes degenerate with the STO conduction band, enabling the injection of electrons into it. This is considered to be the origin of the metal-insulator transition at 4 uc. The process just described is directly related to several quantities accessible via photoemission. The LAO/STO band gaps and band offsets determine what magnitude of field will cause band degeneracy at 4 uc. In a rigid band model, an increase in the energy of the LAO valence band will be reflected in a shift of the LAO core levels relative to STO levels. In addition, as the field causes the binding energies of the LAO layers to differ from one another, the composite LAO peak will broaden.

The LAO/STO valence-band offset is determined using the linear Kraut method.[23] A core-level–valence-band-edge separation is measured for reference samples of the materials on both sides of the interface, which is then used to deduce the band offset from core-level separations measured for the interface sample. Using the Sr $3d_{5/2}$-La $4d_{5/2}$ separation in the annealed TiO_2-terminated 2 uc sample to extract the band-edge offset, we find that the STO valence band is 0.35 ± 0.18 eV above the LAO valence band, as illustrated in Fig. 2. Given the band offset and experimental band gaps,[21,22] an internal field of 1.15 ± 0.06 V/uc is required for the metal-insulator transition to occur at 4 uc thickness.
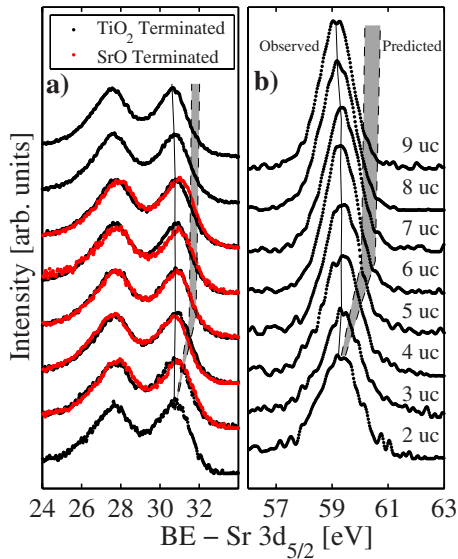
FIG. 3. (Color online) (a) La $4d$ and (b) Al $2p$ photoemissions in annealed samples. To cancel out charging and surface photovoltage effects, the x axis is the binding energy relative to the Sr $3d_{5/2}$ peak in the same sample. The thin solid line tracks the observed peak center, while gray bands follow the range of predicted shifts of the peak, according to the polar catastrophe picture for the TiO$_2$-terminated case. The predicted range is set by built-in fields of 0.6 and 0.9 V/uc taken from Refs. 7 and 8. The upward shift expected to lead to the metal-insulator transition is not observed. Curves are shifted vertically for clarity.

This value is larger than theoretical estimates. In the following, we use field values from theoretical calculations to compare with experiment and show that even these smaller fields are not compatible with measured data.

The Sr $3d_{5/2}$-(La $4d_{5/2}$, Al $2p$) separations in samples after oxygen annealing (Fig. 3) have little dependence on thickness suggesting flat LAO bands. We simulate the effect of a built-in field by examining a composite emission peak, created by summing peaks representing emission from each LAO unit cell (Fig. 2). Each single layer emission energy is shifted by the predicted built-in potential and attenuated according to the depth of the layer. The center and width of the composite peak are then compared with experiment. The prediction of the polar catastrophe scenario for the TiO$_2$-terminated case (gray band in Fig. 3) is a strong upward shift of LAO bands until the metal-insulator transition, followed by a gentler rise. This trend is not observed in the data. The same behavior is observed when using separations of film levels from the Ti $2p$ peak. It is interesting to see that the measured value of the Sr-La separation is almost independent of termination, implying that the transport properties are not controlled by the LAO/STO offset. The polar catastrophe scenario should also cause a large broadening of the film peak before the metal-insulator transition, followed by a small decrease in width after the transition, as a constant potential drop is spread out over more layers. However, the La and Al levels do not change their widths. Comparing the predicted broadening of the La $4d_{5/2}$ peak (Fig. 4) with the observed width indicates again the LAO bands are flat. We note that this analysis method cannot extract the position of
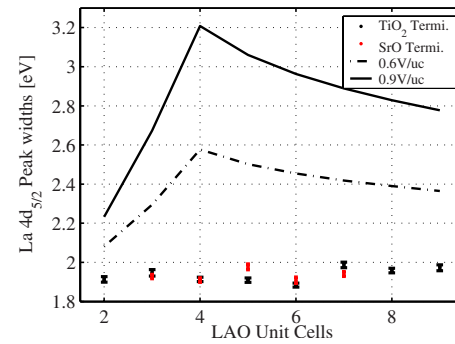

FIG. 4. (Color online) FWHM of La $4d_{5/2}$ peak in annealed samples. Lines follow the expected broadening of the peak, according to the polar catastrophe picture for the TiO$_2$-terminated case. Predicted built-in field magnitudes are taken from Refs. 7 and 8. Broadening in the emission peak due to the potential variation across the film is not observed. No dependence on thickness or termination is observed, and the width is similar to that observed in thick LAO films.

bands relative to the Fermi level because of possible charging. However, it can detect shifts of film and substrate levels relative to each other, which is the key feature of polar catastrophe.

It is of interest to see if there is any difference in electronic structure between the two substrate terminations, reflecting the difference in transport properties. Before oxygen annealing, the Sr $3d_{5/2}$-La $4d_{5/2}$ peak separations show a trend that strongly depends on substrate termination. Figure 5 demonstrates the evolution of the separation with thickness. The substrate is conducting before annealing, making absolute peak centers meaningful, thus allowing us to verify that the change in separation is due to the La peak moving, while the Sr one does not move. Assuming a uniform field in the film, the systematic shift corresponds to fields of 0.06 and 0.14 V/uc (TiO$_2$ and SrO terminated). In the TiO$_2$-terminated case, the film bands are bent downward
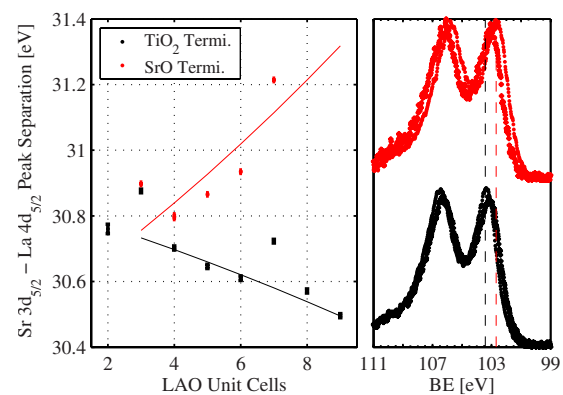

FIG. 5. (Color online) Left: La $4d_{5/2}$-Sr $3d_{5/2}$ separation in as-grown samples. After 3 uc thickness the two terminations diverge. The solid lines track simulated peak positions when the band bending in the LAO is caused by constant fields of 0.06 and 0.14 V/uc for TiO$_2$- and SrO-terminated cases, respectively. Right: La $4d$ levels in Ti-terminated (black, bottom) samples, 4 and 9 uc samples. 4 and 7 uc samples, Sr terminated (red, top). The vertical lines cross the centers of the 9 and 7 uc La $4d_{5/2}$ peaks.

away from the interface, and the opposite sense for the SrO termination. This corresponds to a negative sheet charge at the interface for the TiO_2-terminated case, contrary to the expectation from an uncompensated LaO plane, which has a formal charge of +1. The same field values are found for the Sr $3d_{5/2}$-Al $2p$ separation, verifying this to be an electrostatic rather than chemical shift. The band offsets, however, do not have a strong dependence on termination and do not change upon annealing.

The change in electronic structure with annealing hints that effects other than simply filling of oxygen vacancies in the STO substrate may be important. One effect of annealing on TiO_2-terminated interfaces is the decharging of interface states. The field in the as-grown samples can be due to a negative sheet charge at the buried interface. As the Fermi level is pushed down by annealing, electrons leave interface states, reducing the amount of negative charge present. Another possible effect that can explain the observed transport properties is mixing across the interface being promoted by annealing. Intermixing in annealed LAO/STO interfaces was reflected in cross-section transmission electron microscopy results,[10] which show increased interface roughening in TiO_2-terminated interfaces. Interestingly, in the same study an electron energy loss spectroscopy scan of the SrO-terminated interfaces showed that the energy levels of the different layers of LAO are equal, indicating that no field exists in the polar oxide. A percolative origin for the metal-insulator has been recently suggested,[12] which does not require a polar catastrophe to occur.

In this work, both extrinsic and intrinsic mechanisms for metallic conductivity in LAO/STO were examined. Transport measurements of MBE-grown films demonstrate termination dependence and metal-insulator transition, showing that the origin of this behavior is not unique to a particular growth method. Experimentally determined band offsets require the built-in field to be 1.15 ± 0.06 V/uc for the metal-insulator transition to occur at the experimental thickness of 4 uc. However, photoemission does not find evidence for a field of even the lowest magnitude of theoretical estimates within the polar catastrophe picture. This result requires one to consider mechanisms other than polarization doping. These may arise from an interface that is not abrupt, as hinted by previous experimental observations.[10–12,15]

*yaron.segal@yale.edu

[1] S. A. Pauli and P. R. Willmott, J. Phys.: Condens. Matter **20**, 264012 (2008).

[2] J. W. Reiner, F. J. Walker, and C. H. Ahn, Science **323**, 1018 (2009).

[3] S. Thiel, G. Hammerl, A. Schmehl, C. W. Schneider, and J. Mannhart, Science **313**, 1942 (2006).

[4] A. Ohtomo and H. Y. Hwang, Nature (London) **427**, 423 (2004).

[5] W. Siemons, G. Koster, H. Yamamoto, T. H. Geballe, D. H. A. Blank, and M. R. Beasley, Phys. Rev. B **76**, 155111 (2007).

[6] Z. S. Popović, S. Satpathy, and R. M. Martin, Phys. Rev. Lett. **101**, 256801 (2008).

[7] J. Lee and A. A. Demkov, Phys. Rev. B **78**, 193104 (2008).

[8] C. Cen, S. Thiel, G. Hammerl, C. W. Schneider, K. E. Andersen, C. S. Hellberg, J. Mannhart, and J. Levy, Nature Mater. **7**, 298 (2008).

[9] K. Janicka, J. P. Velev, and E. Y. Tsymbal, Phys. Rev. Lett. **102**, 106803 (2009).

[10] N. Nakagawa, H. Y. Hwang, and D. A. Muller, Nature Mater. **5**, 204 (2006).

[11] P. R. Willmott, S. A. Pauli, R. Herger, C. M. Schlepütz, D. Martoccia, B. D. Patterson, B. Delley, R. Clarke, D. Kumah, C. Cionca, and Y. Yacoby, Phys. Rev. Lett. **99**, 155502 (2007).

[12] A. S. Kalabukhov, Yu. A. Boikov, I. T. Serenkov, V. I. Sakharov, V. N. Popok, R. Gunnarsson, J. Borjesson, N. Ljustina, E. Olsson, D. Winkler, and T. Claeson, Phys. Rev. Lett. **103**, 146101 (2009).

[13] V. E. Henrich, G. Dresselhaus, and H. J. Zeiger, Phys. Rev. B **17**, 4908 (1978).

[14] A. Rizzi, R. Lantier, F. Monti, H. Lüth, F. Della Sala, A. Di Carlo, and P. Lugli, J. Vac. Sci. Technol. B **17**, 1674 (1999).

[15] M. Sing *et al.*, Phys. Rev. Lett. **102**, 176805 (2009).

[16] K. Yoshimatsu, R. Yasuhara, H. Kumigashira, and M. Oshima, Phys. Rev. Lett. **101**, 026802 (2008).

[17] D. F. Mullica, C. K. C. Lok, H. O. Perkins, and V. Young, Phys. Rev. B **31**, 4039 (1985).

[18] S. Tanuma, C. J. Powell, and D. R. Penn, Surf. Interface Anal. **21**, 165 (1994).

[19] J. W. Reiner, A. Posadas, M. Wang, T. P. Ma, and C. H. Ahn, Microelectron. Eng. **85**, 36 (2008).

[20] J. W. Reiner, A. Posadas, M. Wang, M. Sidorov, Z. Krivokapic, F. J. Walker, T. P. Ma, and C. H. Ahn, J. Appl. Phys. **105**, 124501 (2009).

[21] Y. Y. Mi, Z. Yu, S. J. Wang, P. C. Lim, Y. L. Foo, A. C. H. Huan, and C. K. Ong, Appl. Phys. Lett. **90**, 181925 (2007).

[22] S. G. Lim, S. Kriventsov, T. N. Jackson, J. H. Haeni, D. G. Schlom, A. M. Balbashov, R. Uecker, P. Reiche, J. L. Freeouf, and G. Lucovsky, J. Appl. Phys. **91**, 4500 (2002).

[23] E. A. Kraut, R. W. Grant, J. R. Waldrop, and S. P. Kowalczyk, Phys. Rev. Lett. **44**, 1620 (1980).